HHS Public Access

Author manuscript

*Dev Biol*. Author manuscript; available in PMC 2018 August 01.

Published in final edited form as:

*Dev Biol*. 2017 August 01; 428(1): 188–203. doi:10.1016/j.ydbio.2017.06.003.

# Planar cell polarity-dependent and independent functions in the emergence of tissue-scale hair follicle patterns

**Maureen Cetera**[a], **Liliya Leybova**[a], **Frank W. Woo**[a], **Michael Deans**[b,c], and **Danelle Devenport**[a,*]

[a]Department of Molecular Biology, Princeton University, Princeton, NJ, USA

[b]Department of Surgery, Division of Otolaryngology, University of Utah School of Medicine, Salt Lake City, UT, USA

[c]Department of Neurobiology & Anatomy, University of Utah School of Medicine, Salt Lake City, UT, USA

## Abstract

Hair follicles of the mammalian epidermis display local order and global alignment, a complex pattern instructed by the core planar cell polarity (PCP) pathway. Here we address the contributions of core PCP genes, Van Gogh-like and Frizzled, to the establishment, local refinement, and global order of embryonic and postnatal hair follicles. We find that, similar to Fz6 mutants, the disordered hair patterns of Vangl2 mutants are refined over time and eventually corrected. In both mutants, we find that tissue-level reorientation occurs through locally coordinated follicle rotation at stereotyped locations. Strikingly, Vangl2 and Fz6 mutant follicles collectively rotate with opposing directionalities, suggesting that redundant core PCP signals contribute to their directed realignment. Consistently, global follicle alignment is not restored upon conditional ablation of both Vangl1 and Vangl2 genes. Instead, spatially distinct patterns of whorls and crosses emerge and persist even after a complete cycle of hair follicle regeneration. Thus, local refinement of hair follicles into higher order patterns can occur independently of the core PCP system, however, their global alignment with the body axes requires PCP function throughout morphogenesis, growth and regeneration.

### Keywords

Planar cell polarity; Hair follicles; Epidermis; Celsr1; Vangl2; Fz6

## 1. Introduction

The skin of mammals is decorated and protected by a coat of highly ordered body hairs that point in a uniform orientation over the skin surface. Mammalian hairs derive from hair follicles, complex multicellular miniorgans that produce hair and regenerate throughout life.

*Corresponding author. danelle@princeton.edu (D. Devenport).

**Appendix A. Supplementary material**

Supplementary data associated with this article can be found in the online version at http://dx.doi.org/10.1016/j.ydbio.2017.06.003.

Each hair follicle in its fully developed form is comprised of hundreds of epithelial cells organized in concentric layers that are embedded within and ensheathed by stromal cells of the underlying dermis (Schneider et al., 2009). Although hair follicles are spatially separated from one another by interfollicular epithelial cells and dermal fibroblasts, they display remarkable local coordination and global order, representing a striking yet complex example of planar cell polarity (PCP) (Devenport and Fuchs, 2008; Guo et al., 2004). While it is known that a highly conserved 'core' PCP pathway acts during embryogenesis to direct the polarity pattern of murine hair follicles, the temporal and spatial requirements of core PCP genes during hair follicle morphogenesis, growth and postnatal cycling remain unclear (Chang et al., 2016; Devenport and Fuchs, 2008; Wang et al., 2010). Here we address the contributions of the core PCP genes, Van Gogh-like and Frizzled, to the establishment, local refinement, and global order of embryonic and postnatal hair follicles.

PCP orients diverse cellular structures across a wide range of tissues and organisms. It is best understood in simple epithelia such as the *Drosophila* wing blade where PCP orients polarity at the level of individual cells (Adler, 2012; Devenport, 2016). Based on studies primarily in the *Drosophila* wing, it is generally understood that membrane-associated core PCP proteins asymmetrically localize at cell junctions where they interact intercellularly to form asymmetric bridges. Frizzled (Fz) and Flamingo (Fmi, Celsr in vertebrates) on one side of the junction interact with Van Gogh (Vang, Vangl in vertebrates) and Fmi on the opposing interface (Usui et al., 1999; Lawrence et al., 2004; Chen et al., 2008; Strutt and Strutt, 2008; Wu and Mlodzik, 2008; Struhl et al., 2012). Intracellularly, Vang and Fz proteins act antagonistically through their cytoplasmic binding partners to reinforce polarity within a cell. Global, tissue-level directional cues bias the asymmetric localization of core PCP proteins, which in turn act on downstream cytoskeletal and trafficking effectors to generate the structural polarity of individual cells (Devenport, 2014; Goodrich and Strutt, 2011; Vladar et al., 2009). How these principals apply to much more complex multicellular structures, like mammalian hair follicles, is poorly understood.

Developing hair follicles gain their first signs of asymmetry during embryogenesis, shortly after hair follicle placodes first invaginate into the underlying dermis (Devenport and Fuchs, 2008). Hair follicle placodes form an acute and unidirectional tilt that is oriented in an anterior direction over most of the body surface. Proliferation drives further anterior-directed growth as follicles maintain and refine their anterior-biased position. Following differentiation into several concentric and specialized cell layers, hair follicles produce keratin-rich hairs that protrude from the skin surface in a posterior direction (Schneider et al., 2009). Follicles then undergo several rounds of destruction (catagen) and regeneration (anagen) throughout postnatal life (Alonso and Fuchs, 2006), yet maintain their precise and ordered planar polarized pattern. Whether continued input from the core PCP pathway is required to maintain and refine the postnatal hair pattern is not known.

The core PCP genes Vangl2, Celsr1, and Fz6 are required for hair follicle alignment where they act during early stages of hair follicle morphogenesis to drive the anterior-directed tilt of hair follicle placodes (Chang et al., 2016; Devenport and Fuchs, 2008; Guo et al., 2004; Ravni et al., 2009; Wang et al., 2010). Prior to hair follicle downgrowth, Vangl2, Celsr1, and Fz6 proteins become asymmetrically localized within basal epidermal cells – progenitor

cells that give rise to hair follicles (Fig. 1A; Devenport and Fuchs, 2008). Vangl2 preferentially localizes to the anterior side of basal cells, while Fz6 becomes enriched on the posterior. Celsr1, an atypical cadherin, localizes to both anterior and posterior sides, where it is thought to bridge Vangl2 and Fz6 between adjacent cells. PCP protein asymmetry prefigures the orientation of hair follicles, which tilt and elongate in the direction of Vangl2 localization (Devenport and Fuchs, 2008; Devenport et al., 2011). In the absence of Vangl2 or Celsr1 function, hair placodes invaginate perpendicular to the epithelium and point straight downward, whereas Fz6 mutant follicles emerge at random orientations (Chang et al., 2016; Devenport and Fuchs, 2008; Wang et al., 2010).

During postnatal stages, hair follicle angles become increasingly coordinated, both locally and globally, to align precisely with the anterior-posterior axis. Strikingly, this process of postnatal refinement occurs independently of Fz6 function (Wang et al., 2006, 2010). In Fz6 KO mice, the initially disordered pattern of hair follicle angles corrects over time, whereby at postnatal day 21, the normal hair follicle pattern is completely restored (Chang and Nathans, 2013). The ability of hair follicles to rotate within the dermis and correct their orientations highlights remarkable plasticity of adult hair follicles. However, hair follicle refinement has not been observed in any other core PCP mutant to date, raising the question of whether this phenomenon is unique to the Fz6 allele. There are over 10 different Fz homologs present in the mouse genome, and deletion of Fz6 produces only mild defects compared to other PCP mutants (Wang et al., 2016). Thus, it is unclear whether redundant core PCP cues instruct the postnatal hair follicle pattern in Fz6 mutants, or whether a parallel PCP system, such as the Fat-Dachsous- Four-jointed system (Matis and Axelrod, 2013), functions postnatally to correct hair follicle alignment.

Here, by characterizing tissue-wide patterns of cellular and hair follicle polarity, we define the core PCP-dependent and independent events in the establishment and refinement of the mammalian hair pattern. We find that, although Vangl2 and Fz6 are required for the initial polarization and alignment of nascent hair follicles, the disordered hair patterns of both PCP mutants are refined and eventually corrected, through stereotyped and locally coordinated rotational patterns. Strikingly, Vangl2 and Fz6 mutant follicles collectively rotate with opposing directionalities, suggesting that realignment occurs through redundant core PCP signals. Surprisingly, follicle rotation is not prefigured by PCP protein asymmetry in the interfollicular epidermis. Finally, eliminating all Vangl function through conditional ablation of both Vangl1 and Vangl2 genes in the skin yields a distinct global hair pattern of highly reproducible whorls and crosses that persists during follicle growth and regeneration. These results demonstrate that the local, collective rotation of hair follicles into higher order patterns is a largely PCP-independent process. However, the directional sensing mechanisms that enable follicles to align with the global body axes require continued input from the core PCP pathway.

## 2. Methods

### 2.1. Mouse lines and breeding

All procedures involving animals were approved by Princeton University's Institutional Animal Care and Use Committee (IACUC). Mice were housed in an AAALAC-accredited

facility in accordance with the Guide for the Care and Use of Laboratory Animals. Please see Table 1 for full genotypes.

### 2.2. Embryo preparation and whole-mount immunostaining

For embryonic immunostaining, embryos were dissected in PBS and fixed in 4% paraformaldehyde. E15.5 embryos were fixed for 1 h and e17.5 embryos were fixed for 2 h following decapitation. Dissected back skin was blocked for 1 h at room temperature or overnight at 4 °C in 2% normal goat serum, 2% normal donkey serum, 1% bovine serum albumin and 1% fish gelatin in PBT2 (PBS with 0.2% Triton X-100). Skins were incubated with primary antibodies in blocking solution overnight at 4 °C. Skins were washed in PBT2 and incubated with secondary antibodies for 2 h at room temperature or overnight at 4 °C in PBT2. Samples were mounted in Prolong Gold. The following primary antibodies were used: guinea pig anti-Celsr1 (1:1000, D. Devenport), rat anti-E-Cadherin (1:1000, DECMA-1, Thermo Pierce), rat anti-Vangl2 (1:100, 2G4, Millipore), rabbit anti-Vangl2 (1:500, Millipore, 2668504) (pan-Vangl) (Belotti et al., 2012). Alexa Fluor-488,-555, and −647 secondary antibodies were used at 1:1000. Images were acquired on an inverted Nikon A1 or A1R-Si confocal microscope controlled by NIS Elements software using a Plan Apo 60/1.4NA or 40/ 1.3NA oil immersion objective. ImageJ and Photoshop were used for image processing.

### 2.3. Quantification of embryonic hair follicle orientation

Full embryonic back skin images were acquired by tiling 20x images obtained on a Nikon Eclipse Ti epifluorescence microscope using a Plan Apo 20/0.75NA objective. NIS Elements software was used to tile and measure follicle angles. A reference angle was set along the anterior posterior axis and a line was drawn over each follicle towards its base. The difference between the two angles provides the orientation of the hair follicle.

### 2.4. Sample preparation and quantification of postnatal hair follicle orientation

Skin was prepared as previously described (Chang et al., 2014). After euthanasia, animals over 7 days old were shaved and hair was removed using Nair. Dorsal back skin was dissected from P2-P39 animals and pinned to solidified paraffin in a petri dish with the dermis facing up and fixed overnight at 4 °C. Fixed skins were washed in PBS and dehydrated over consecutive days in 70%, 95%, and 100% ethanol. Dehydrated skins were placed between microscope slides in a glass petri dish to keep them flat. BABB (2:1 ratio of benzyl benzoate and benzyl alcohol) was added to clear the tissue overnight. Brightfield images were acquired on a Nikon SMZ1270 dissecting scope using a Plan Apo 0.5x objective and a Nikon Digital Sight Fi1 camera. Samples were illuminated from below the dish and images were taken with 3–8x magnification. Whole backskin images were obtained by stitching together high magnification images with Photomerge in Photoshop.

To account for differences in animal size, each high magnification image was cropped to the same anterior-posterior and lateral region and scaled to 2706 × 1436 pixels. The scaled images were inverted and the color survey was produced using the ImageJ plugin, OrientationJ, with a 5-pixel Gaussian window. Tissue-level alignment was determined as previously described (Cetera et al., 2014). Briefly, the inverted image was segmented into a

38×74 grid containing windows that overlap with their neighbors by 50%. In each window the local orientation of the hair follicles was determined as an angle orthogonal to the principle direction of the 2D FFT of that window. This creates an angle matrix with values that correspond to the window position. All angles were combined across tissues of the same genotype and the relative frequency of the angles was plotted in a histogram. Data were separated by their anterior-posterior positions and plotted to show positional trends across the tissue. Because animals are born with all of their hair follicles, the window size for each scaled image would contain approximately the same number of hair follicles from stage P2-P7 (approximately 2–5).

### 2.5. Postnatal tissue clearing and immunostaining

Backskins were dissected and fixed as described above. 0.5 × 1 cm sections were cut away for further processing. Samples were processed and stained using the iDISCO protocol as previously described (Renier et al., 2014). Briefly, fixed samples were dehydrated in a graded methanol series, bleached overnight at 4 °C in methanol with 5% $H_2O_2$ and 20% DMSO. Tissue was rehydrated and permeabilized in 0.3 M glycine in PBT3 (PBS with 0.3% Trition X-100) with 20% DMSO for 2 days at 37 °C. Samples were blocked in PBT3 with 10% DMSO, 3% NGS and 3% NDS for 4 days at 37 °C. Samples were washed in PBS with 0.2% Tween-20 and incubated with primary antibodies in PBS with 0.2% Tween-20, 5% DMSO, 3% NDS for 5–10 days at 37 °C. Primary antibody concentrations were slightly increased: anti-Celsr1 (1:800), anti-E-Cadherin (1:800). Samples were washed all day in PBS with 0.2% Tween-20 and then incubated with secondary antibodies in PBS with 0.2% Tween-20% and 3% NDS for 3 days at 37 °C. Samples were washed again and dehydrated in a graded methanol series followed by two 15 min incubations in Dichloromethane. Tissues were cleared and stored in dibenzylether (DBE). An imaging chamber was made by making a ring of vacuum grease on a microscope slide and placing the cleared tissue in the center of the ring with a drop of DBE. A coverslip was added with poster putty placed at the corners to secure the chamber. Images were acquired on an inverted Nikon A1 or A1R-Si confocal microscope controlled by NIS Elements software using a Plan Apo 60/1.4NA or 40/1.3NA oil immersion objective. ImageJ and Photoshop were used for image processing.

### 2.6. Quantification of Celsr1 polarity

Celsr1 polarity was calculated using Packing Analyzer V2 software as previously described (Aigouy et al., 2010). The software calculates the axis and magnitude (nematic order) of juntional polarity. Cells were segmented using the E-Cadherin signal when possible or the Celsr signal. Celsr polarity within a cell was normalized by the corresponding average cell boundary Celsr intensity as previously described (Aw et al., 2016). Data were plotted in a circular histogram using the polar plot function in Matlab. Histograms were weighted by the average magnitude of polarity in each bin to reflect both the angle and strength of polarity. The magnitude ($M_P$) and orientation of average Celsr polarity was overlaid as a line on top of the histogram where the length of the line and its orientation reflects the magnitude and direction of Celsr polarity.

### 2.7. Statistical analysis for Celsr1 polarity

Each distribution of Celsr1 asymmetry was subjected to a permutation test to determine whether or not the distribution could be achieved at random by resampling the data. Nematic tensor values corresponding to each cell across samples were randomly permuted 10,000 times, and for each permutation, the magnitude of the average polarity ($M_p$) was calculated. The P-value is given by the proportion of permutations with magnitudes greater than or equal to half a standard deviation below that of the original data. A distribution was considered significant if $P \leq 0.01$ (Aw et al., 2016).

## 3. Results

### 3.1. Tissue-level hair follicle alignment is restored in a Vangl2 and Fz6-independent manner

Previous studies demonstrated that despite the initially random pattern of hair follicle orientations in Fz6 KO embryos, follicle alignment is eventually restored during postnatal stages (Chang and Nathans, 2013; Wang et al., 2010). Fz6 mutant follicles rotate up to 180 degrees to align along the A-P axis, suggesting the existence of additional directional cues that instruct postnatal follicle realignment (Wang et al., 2010). It is possible that other Fz genes provide this postnatal function, as several other Fz genes are expressed in the postnatal skin (Sennett et al., 2015). To address whether the core PCP pathway directs the postnatal hair pattern, we focused on the Vangl genes as there are only two, Vangl1 and Vangl2, in the mouse genome. Deletion of Vangl2 is embryonic lethal (Song et al., 2010; Yin et al., 2012), so we conditionally deleted the Vangl2 gene in the skin epithelium using K14-Cre (henceforth referred to as Vangl2 cKO) (Copley et al., 2013; Vasioukhin et al., 1999; Yin et al., 2012).

We and others have previously shown that mutations affecting Vangl2 cause global disorganization of hair follicles during embryonic stages (Chang et al., 2016; Devenport and Fuchs, 2008; Wang et al., 2010). As expected, when Vangl2 was conditionally deleted in the skin epithelium using K14-Cre, hair follicle angles were highly disordered at postnatal day 2 (P2) (Fig. 1B,D; Chang et al., 2016). To quantify the defect, whole backskins were segmented into overlapping windows and a two-dimensional fast Fourier transform was used to determine the local orientation of the hair follicles in a given window (Cetera et al., 2014). Compared to control littermates, where the growing end of each follicle pointed anteriorly and follicle shafts aligned along the anterior-posterior axis, Vangl2 cKO follicle angles were highly disordered. The Vangl2 cKO hair pattern was similar to, but more severe than Fz6 KO full body mutants at the equivalent stage (Fig. 1B,D). To visualize the local order and global pattern of the thousands of follicles across the entire dorsal surface of the body, tiled images of dorsal backskins were acquired and processed using OrientationJ to color-code individual follicles according to their directionality (Puspoki et al., 2016; Fig. 2). This method highlighted the distribution of orientations among neighboring follicles of Vangl2 cKO and Fz6 KO mutants at P2, as well as the regional differences in hair patterns along the anterior-posterior axis. Disorder was especially pronounced in caudal regions of Vangl2 cKO and Fz6 KO mutants, whereas follicle orientations were more modestly affected rostrally (Fig. 2A – C).

Remarkably, at P7, Vangl2 cKO and Fz6 KO follicle orientations were comparable to control littermates, suggesting the initially disordered pattern had corrected over time (Fig. 1C and E). Across the dorsal skin, Vangl2 cKO and Fz6 KO follicles displayed a high degree of local order and were globally aligned along the A-P axis (Fig. 2D–F). PCP mutants were largely indistinguishable from their wild type or heterozygous littermates with the exception of prominent hair whorls on the distal hindlimbs of mutant, but not control mice. Interestingly, limb whorls persisted beyond P39, suggesting that in contrast to dorsal skin, limb hair patterns do not correct over time.

### 3.2. Hair follicles of Vangl2 and Fz6 mutants display opposing rotational patterns

The normal, globally aligned hair pattern observed in PCP mutants at P7 suggested that initially disordered follicles rotate to align with the A-P axis. If true, intermediate hair patterns with increasing order should be observable between days P2 and P7 of development. Therefore, we quantified hair follicle angles across the entire dorsal skin surface of P4 mice and found that PCP mutant follicles correct, they pass through highly reproducible and stereotyped intermediate patterns. Follicle angles of Vangl2 cKO and Fz6 KO mice were locally coordinated but globally misaligned, generating characteristic swirling hair patterns across the dorsal epidermis (Figs. 3 and 4). The degree of local coordination between neighboring follicles appeared similar between Vangl2 and Fz6 mutants (Fig. 4), but strikingly, their global patterns were distinct and, in some areas, directionally opposed. In Vangl2 mutants, the growing anterior ends of follicles pointed inwards toward the midline (Fig. 4C), whereas Fz6 mutant follicles pointed away (Fig. 4E). This phenotype was highly reproducible across individuals (Fig. 4D, F; Supplementary Fig. 1) and suggested that Fz6 and Vangl2 mutant follicles realign by rotating in opposite directions. It should be noted that the stereotyped and reproducible pattern we observe in Fz6 mutants is distinct from the hair patterns previously described, a difference we attribute to genetic background (Wang et al., 2006, 2010). In particular, the presence of the ridge allele or other modifiers in the original Fz6 KO line may have contributed to the more random hair pattern and to the slower rate of hair follicle refinement than we observe in our backcrossed line (Chang et al., 2015). Together, our results demonstrate that during postnatal stages, hair follicles are locally coordinated and globally aligned independently of Vangl2 and Fz6. However, the opposing rotational patterns observed in Vangl2 and Fz6 mutants suggests that realignment might be directed though residual core PCP function.

### 3.3. Hair follicle polarity is uncoupled from PCP protein asymmetry during realignment

The reorganization of PCP mutant follicles into the correct global pattern raised the question of whether PCP protein localization is asymmetric in the postnatal epidermis, and if so, whether polarity aligns with the direction of rotating hair follicles. During embryogenesis, hair follicle polarization is preceded by asymmetric Celsr1 protein localization in the interfollicular epidermis (Devenport and Fuchs, 2008). Moreover, the direction of Celsr1 asymmetry across different body regions strongly correlates with hair follicle orientation (Aw et al., 2016; Devenport and Fuchs, 2008; Devenport et al., 2011). Because Celsr2 does not asymmetrically localize in basal cells (data not shown) and Celsr3 is not expressed (Sennett et al., 2015), Celsr1 is a reliable indicator of PCP protein asymmetry in skin.

We hypothesized that postnatal follicle patterns are prefigured by PCP asymmetry in the interfollicular epidermis, as are actin pre-hairs in the *Drosophila* wing (Strutt, 2001). However, due to technical limitations caused by tissue thickness and autofluorescence, the distribution of PCP proteins in the postnatal skin has never been visualized. Therefore, we adapted tissue-clearing methods (iDISCO) to enable immunofluorescent imaging of epidermal whole mounts (Renier et al., 2014) and quantified PCP asymmetry by calculating the nematic order of the integrated fluorescence intensity values of Celsr1 at cell borders (Aigouy et al., 2010; Aw et al., 2016). In control mice at P4, Celsr1 was asymmetrically distributed towards the anterior and posterior sides of basal cells, correlating with the axis of hair follicle alignment (Fig. 5A – C). By contrast, Celsr1 asymmetry was strongly reduced or randomized in Vangl2 cKO and Fz6 KO mutants, and was largely uncorrelated with the local orientation of follicles (Fig. 5A – C). For example, Fig. 5B shows a representative region of Vangl2 cKO epidermis where hair follicles are oriented at roughly 45 degree angles. However, Celsr1 asymmetry in the surrounding epidermis is highly disordered and does not align with nearby follicles. These results indicated that hair follicle realignment occurs independently of Celsr1 asymmetry in the epidermis, demonstrating that, at least in postnatal stages, hair follicle orientation and epidermal PCP can be uncoupled.

To determine whether PCP mutant hair follicle orientations correlate with epidermal polarity during embryogenesis when follicle polarity is initially established, Celsr1 asymmetry and hair follicle angles were quantified in control, Vangl2 cKO and Fz6 KO epidermis at embryonic stages where this relationship has not yet been investigated. Vangl2 cKO embryos display variable hair follicle orientations at E17.5 (Fig. 6A and B), similar to the previously described phenotype of Fz6 KO (Fig. 6A and B; Chang et al., 2016; Wang et al., 2010). Whereas the angular distribution of Celsr1 polarity closely correlated with the orientation of hair follicles in control embryos, this relationship was not observed in Vangl2 cKO or Fz6 KO embryos, where Celsr1 asymmetry was strongly reduced (Fig. 6C and D). We observed a similar reduction of Celsr1 polarity in PCP mutants at E15.5, the time when hair placodes normally acquire the first signs of an anterior-directed bend (Fig. 7; Devenport and Fuchs, 2008). At E15.5, Fz6 KO and Vangl2 cKO follicles often lacked an anterior bend, or were polarized in random orientations (Fig. 7A–C). Notably, these phenotypes are less severe than the previously reported phenotypes of dominant negative $Vangl2^{Lp/Lp}$ or $Celsr1^{Crsh/Crsh}$ mutants, suggesting Fz6 KO and Vangl2 cKO embryos retain some epidermal PCP function (Devenport and Fuchs, 2008; Wang et al., 2010). Nevertheless, when Celsr1 asymmetry was quantified in the interfollicular epidermis of Vangl2 cKO and Fz6 KO embryos, polarity was strongly reduced, accumulating more uniformly around the cell cortex compared to the anterior-posterior enrichment found in control embryos (Fig. 7D and E). Occasionally, Celsr1 was weakly polarized in patches of Vangl2 cKO mutant epidermal cells, but the direction of asymmetry was not obviously correlated with the angle of the nearest follicles.

### 3.4. Hair follicles form complex, spatially distinct patterns in the absence of core PCP function

To test whether the core PCP pathway mediates postnatal hair follicle realignment, we generated mice that lacked all four Vangl alleles in the skin epidermis (referred to as Vangl1;

Vangl2 dcKO). As there are only two Vangl genes in the mouse genome, this allelic combination eliminates all Vangl-dependent PCP function. Using Vangl2-specific and pan-Vangl antibodies, we confirmed that by embryonic day E15.5, Vangl proteins levels were eliminated in K14-Cre positive cells (Supplementary Fig. 2; Belotti, 2012). At E15.5, the majority of Vangl1;Vangl2 dcKO hair follicles failed to polarize, growing vertically into the dermis, perpendicular to the epithelial plane (Fig. 8A and B). This phenotype was significantly more severe than either Fz6 KO or Vangl2 cKO embryos (Fig. 6A and B), and mimicked the phenotype observed in Vangl2$^{Lp/Lp}$ mutants (Devenport and Fuchs, 2008; Wang et al., 2010), which carries a dominant negative mutation in Vangl2 that interferes with cell surface delivery of Vangl1 (Yin et al., 2012). Twenty percent of Vangl1; Vangl2 dcKO placodes displayed at least some degree of bending, which could be attributed to a small amount of incomplete Cre-recombination, but more likely reflects the follicles that have begun to undergo rotational movements (see below). As expected, this phenotype was accompanied by a loss of Celsr1 asymmetry in the interfollicular epidermis (Fig. 8C and D).

We then examined Vangl1;Vangl2 dcKO hair coats at postnatal stage P7, the time point at which the hair pattern of Fz6 and Vangl2 single mutants had corrected. In contrast to Fz6 or Vangl2 single mutants, Vangl1;Vangl2 dcKO pups displayed highly stereotyped hair patterns of whorls and crosses (Fig. 9A and B; Supplementary Fig. 3). Each P7 dcKO pup displayed three dorsal hair whorls, one centrally located near the head/neck boundary and two located more posteriorly on either side of the midline. Midway along the A-P axis, body hairs were oriented in a cross shapes centered around the central midline (Fig. 9; Supplementary Fig. 3). This phenotype was highly reproducible across individuals, and formed independently of the amount or spatial distribution of small mosaic patches in K14-Cre activity (Supplementary Fig. 3). In the interfollicular epidermis, Celsr1 failed to polarize, localizing weakly or uniformly at the cell cortex, indicating that rotational movements that coordinate local follicle orientations occur in the absence of PCP protein asymmetry (Fig. 8E and F). These results demonstrate that Vangl genes, and likely the core PCP pathway in general, are dispensable for the local coordination of neighboring follicles into higher order patterns. However, most follicles failed to align with the A-P axis suggesting that Vangl1 and Vangl2 are needed in the epidermis for the interpretation of tissue-level directional cues. Alternatively, perhaps compared to Fz6 or Vangl2 single mutants, the Vangl1;Vangl2 dcKO hair pattern is simply slower to resolve. To test the latter hypothesis, we followed Vangl1;Vangl2 dcKO mice into adult stages and beyond the first complete hair cycle.

### 3.5. Stereotyped hair patterns evolve but fail to globally correct in the absence of core PCP function

Following morphogenesis, hair follicles cycle through repeated rounds of destruction and regeneration. The first round of destruction occurs at approximately P14-P18 of postnatal development and regeneration occurs between P22-P37 (Alonso and Fuchs, 2006). To determine whether Vangl function is needed beyond the first hair cycle, we followed the hair patterns of Vangl1;Vangl2 dcKO mice from P7 to P39. Vangl1;Vangl2 dcKO mice were clearly distinguishable from their littermates beyond P7 due to the scruffy appearance of their hair coats (Fig. 10A). Compared to control littermates, Vangl1;Vangl2 dcKO regenerated follicles at P30 continued to display globally disordered patterns (Fig. 10B and

C), but in some regions the patterns were distinct from those the same animals displayed at P7, suggesting that follicles continually refine their orientations beyond the period of hair follicle morphogenesis. For example, P30 mice displayed two prominent hair whorls along the midline, one rostral, one caudal. In addition, hairs were reversed along much of the lower back converging into a cross at the central midline (Fig. 10C, Supplementary Fig. 4). These results demonstrate that core PCP function is absolutely required for global A-P alignment throughout hair follicle development and regeneration. We also conclude that restoration of body hairs into the normal pattern in Vangl2 cKO mice is mediated by postnatal Vangl1 function.

## 4. Discussion

Wang et al. (2006) first described the unexpectedly dynamic nature of hair follicle orientations, where they observed in Fz6 KO mice that locally coordinated hair patterns emerged from initially disordered states, which eventually correct over time (Chang and Nathans, 2013; Wang et al., 2006, 2010). Given the large number of Fz genes present in the mouse genome, and the relatively weak phenotype of Fz6 knockout mice compared to other core PCP mutants (Devenport and Fuchs, 2008; Wang et al., 2010), it was unclear whether hair follicle refinement was mediated by redundant core PCP function or through the action of an alternative, postnatal PCP pathway such as the Fat-Dachsous-Four-jointed system described in flies and vertebrates. Here we resolve this issue by examining PCP establishment and hair follicle patterning in the absence of core PCP function though conditional deletion of Vangl2 and Vangl1; Vangl2 in the skin epithelium. We show that hair follicles of Vangl-deficient skin rearrange extensively during morphogenesis, growth, and regeneration, assembling into locally ordered patterns of hundreds of neighboring follicles. We conclude that the rotational movements and local interactions driving hair follicle refinement are not only Fz6-independent but are core PCP-independent processes. However, because Vangl-deficient hair patterns persist and even rearrange into new formations following hair follicle regeneration, we conclude that the core PCP pathway is essential for the directional sensing mechanism that aligns hair follicles globally with the body axes.

Compared to *Drosophila*, the repertoire of core PCP genes is expanded in mammals, which have multiple copies of each core component (Goodrich and Strutt, 2011). Duplicate PCP genes have partially overlapping functions in other murine tissues (Boutin et al., 2014; Etheridge et al., 2008; Hua et al., 2014; Song et al., 2010), and this and other studies demonstrate that PCP genes also act redundantly in the skin (Chang et al., 2016). In the embryo, Vangl1 can partially compensate for Vangl2 in placode polarization, as conditional ablation of Vangl2 alone causes a significantly weaker phenotype than deletion of both Vangl gene products. Later during postnatal stages, we show that redundant cues restore the global hair pattern in Vangl2 cKO mutants, and it is Vangl1 which provides this function. Because Fz and Vangl are thought to provide equal but opposing roles in PCP, our findings also imply that additional Fz proteins beyond Fz6 must contribute to PCP in the dorsal epidermis. Interestingly, in the hind limb, disordered hair patterns of Vangl2 and Fz6 single mutants do not correct over time, suggesting these are the sole Vangl and Fz genes that function in the limbs. Alternatively, dorsal backskin may exhibit distinct physical and mechanical properties that allow follicles to refine.

PCP is manifested at two levels in the mammalian epidermis - at the level of individual basal cells through the asymmetric segregation of core PCP components, and at the level of multicellular clusters through the polarization of hair placodes and alignment of postnatal hair follicles (Devenport and Fuchs, 2008). Basal cell and hair follicle polarity are clearly linked by the fact that basal cells are progenitors that give rise to hair placodes, and that the direction of PCP asymmetry in basal cells aligns with the direction of hair follicle growth (Devenport and Fuchs, 2008; Devenport et al., 2011). Additionally, elimination of PCP function in interfollicular epidermal cells alters the polarity of neighboring wild type hair follicles (Devenport and Fuchs, 2008; Chang et al., 2016). To what extent the polarity of basal cells instructs the orientation of hair follicles at different developmental stages, however, was unclear. Using the variable follicle orientations in Fz6 and Vangl2 single mutants to investigate this relationship, we found that, surprisingly, hair follicle orientations did not follow PCP asymmetry in the surrounding epidermis neither at postnatal nor at embryonic stages. In Fz6 mutants, hair placodes polarize and postnatal follicles rotate in the absence of detectable Celsr1 asymmetry, suggesting that polarized localization of PCP components may be dispensable for placode polarization. Alternatively, it may be that only slight asymmetries in PCP distribution, beyond the level we can detect with current imaging and analysis tools, are sufficient to drive bending and rotation of the follicle. In Vangl2 cKO animals, where Celsr1 was asymmetric albeit randomized, follicle orientations were also uncoupled from the polarity of surrounding basal cells. It is possible that the pattern of Celsr1 asymmetry is unstable in PCP mutants, and like the hair follicle pattern, changes orientation over time. If so, the snapshots of Celsr1 asymmetry measured here may not reflect the direction of polarity at the precise moment of hair follicle polarization or rotation. Deciphering the cellular mechanisms by which PCP orients developing follicles will help to resolve this issue. Although follicle polarization may require only low levels of PCP function, their coordinate alignment across the epithelium is more sensitive to PCP levels and correlates with robust PCP protein polarization.

Our tissue-wide analysis of postnatal hair patterns revealed that different PCP mutants produce distinct and stereotyped local arrangements. Notably, Fz6 KO and Vangl2 cKO follicles collectively rotate in opposite directions. This phenomenon resembles the opposing non-autonomous phenotypes of Fz and Vang mutant clones in the *Drosophila* wing (Vinson and Adler, 1997; Taylor et al., 1998). A major distinction, however, is that Fz6 and Vangl2 mutant hair patterns are not caused by mosaicism but result from tissue-wide (or body-wide) removal of gene function. In contrast, tissue-wide removal Fz or Vang function in *Drosophila* wings produces wing hair patterns with highly similar directionalities (Taylor et al., 1998), consistent with the idea that Fz6 KO and Vangl2 cKO epithelia retain some core PCP function. How residual PCP cues control the direction of postnatal follicle rotation is still mysterious.

Despite lacking most, if not all, epidermal core PCP function, Vangl1; Vangl2 dcKO follicles arrange into complex and reproducible locally ordered patterns. Local, swirling polarity patterns are also observed in *Drosophila* PCP mutants (Adler et al., 1998; Gubb and Garcia-Bellido, 1982; Taylor et al., 1998; Vinson and Adler, 1997; Wong and Adler, 1993), and it is thought these patterns emerge in response to additional polarity pathways that, in the absence of core PCP function, are sufficient to generate local order but not global tissue

alignment (Vinson and Adler, 1997; Wong and Adler, 1993). The emergence of large-scale regional hair patterns in the skin of core PCP mutant mice shares features with those observed in *Drosophila* but on a much larger spatial and temporal scale. Like the wing, different areas along the dorsal backskin display unique local hair arrangements. Local patterns emerge along the dorsal epidermis in discrete zones, and the positions of these zones are similar between the different PCP mutants. This suggests that the skin may be organized into distinct compartments each with its own combination of polarity pathways, global polarizing cues, and/or physical properties. In a subset of these compartments, follicles of Vangl2 cKO and Fz6 KO mice rotate in opposite orientations suggesting that compartmental cues bias local hair follicle orientations by intersecting with the core PCP pathway. These results imply that although the skin appears to be a single uniform and continuous tissue, the global cues that direct the PCP pattern, whether graded or mechanical in nature, might be distributed compartmentally. Thus, in the search for global polarizing cues that instruct PCP in the epidermis, we should expect not a single source that is graded across the tissue, but perhaps several regional factors that combine to generate a single, continuously aligned pattern.

## Supplementary Material

Refer to Web version on PubMed Central for supplementary material.

## Acknowledgments

We gratefully acknowledge those who provide mouse lines, technical support, and valuable discussions that contributed to this project. We thank Saori Haigo and Jeremy Reiter for generous donation of Vangl2 and Fz6 alleles in mT/mG backgrounds. Jeremy Nathans kindly provided the Vangl1 floxed mouse line. Beniot Aiguoy developed and distributed Packing Analyzer v2 software for image analysis. Patrick Oakes provided the Matlab script used to quantify postnatal hair follicle orientation. Jean-Paul Borg provided the Vangl2 monoclonal antibody. We thank Laura Murray for assisting in the initial characterization of Vangl2 cKO phenotypes, Katie Little for assistance with genetic crosses and genotyping, and members of the Devenport lab for insightful comments and suggestions. Finally, we thank Gary Laevsky for imaging support and expertise. The Confocal Facility at Princeton University is a Nikon Center of Excellence.

**Funding**

Research reported in this publication was supported by the National Institute of Arthritis and Musculoskeletal and Skin Diseases of the National Institutes of Health under Award Number R01AR066070.

## References

Adler PN. The frizzled/stan pathway and planar cell polarity in the Drosophila wing. Curr. Top. Dev. Biol. 2012; 101:1–31. [PubMed: 23140623]

Adler PN, Charlton J, Liu J. Mutations in the cadherin superfamily member gene dachsous cause a tissue polarity phenotype by altering frizzled signaling. Development. 1998; 125:959–968. [PubMed: 9449678]

Aigouy B, Farhadifar R, Staple DB, Sagner A, Roper JC, Julicher F, Eaton S. Cell flow reorients the axis of planar polarity in the wing epithelium of Drosophila. Cell. 2010; 142:773–786. [PubMed: 20813263]

Alonso L, Fuchs E. The hair cycle. J. Cell Sci. 2006; 119:391–393. [PubMed: 16443746]

Aw WY, Heck BW, Joyce B, Devenport D. Transient tissue-scale deformation coordinates alignment of planar cell polarity junctions in the mammalian skin. Curr. Biol. 2016; 26:2090–2100. [PubMed: 27451904]

Belotti E, Puvirajesinghe TM, Audebert S, Baudelet E, Camoin L, Pierres M, Lasvaux L, Ferracci G, Montcouquiol M, Borg JP. Molecular characterisation of endogenous Vangl2/Vangl1 heteromeric protein complexes. PLoS One. 2012; 7:e46213. [PubMed: 23029439]

Boutin C, Labedan P, Dimidschstein J, Richard F, Cremer H, Andre P, Yang Y, Montcouquiol M, Goffinet AM, Tissir F. A dual role for planar cell polarity genes in ciliated cells. Proc. Natl. Acad. Sci. USA. 2014; 111:E3129–E3138. [PubMed: 25024228]

Cetera M, Ramirez-San Juan GR, Oakes PW, Lewellyn L, Fairchild MJ, Tanentzapf G, Gardel ML, Horne-Badovinac S. Epithelial rotation promotes the global alignment of contractile actin bundles during Drosophila egg chamber elongation. Nat. Commun. 2014; 5:5511. [PubMed: 25413675]

Chang H, Cahill H, Smallwood PM, Wang Y, Nathans J. Identification of Astrotactin2 as a genetic modifier That Regulates the Global Orientation of Mammalian Hair Follicles. PLoS Genet. 2015; 11:e1005532. [PubMed: 26418459]

Chang H, Nathans J. Responses of hair follicle-associated structures to loss of planar cell polarity signaling. Proc. Natl. Acad. Sci. USA. 2013; 110:E908–E917. [PubMed: 23431170]

Chang H, Smallwood PM, Williams J, Nathans J. The spatio-temporal domains of Frizzled6 action in planar polarity control of hair follicle orientation. Dev. Biol. 2016; 409:181–193. [PubMed: 26517967]

Chang H, Wang Y, Wu H, Nathans J. Flat mount imaging of mouse skin and its application to the analysis of hair follicle patterning and sensory axon morphology. J. Vis. Exp. 2014:e51749. [PubMed: 24999071]

Chen WS, Antic D, Matis M, Logan CY, Povelones M, Anderson GA, Nusse R, Axelrod JD. Asymmetric homotypic interactions of the atypical cadherin flamingo mediate intercellular polarity signaling. Cell. 2008; 133:1093–1105. [PubMed: 18555784]

Copley CO, Duncan JS, Liu C, Cheng H, Deans MR. Postnatal refinement of auditory hair cell planar polarity deficits occurs in the absence of Vangl2. J. Neurosci. 2013; 33:14001–14016. [PubMed: 23986237]

Devenport D. The cell biology of planar cell polarity. J. Cell Biol. 2014; 207:171–179. [PubMed: 25349257]

Devenport D. Tissue morphodynamics: translating planar polarity cues into polarized cell behaviors. Semin. Cell Dev. Biol. 2016; 55:99–110. [PubMed: 26994528]

Devenport D, Fuchs E. Planar polarization in embryonic epidermis orchestrates global asymmetric morphogenesis of hair follicles. Nat. Cell Biol. 2008; 10:1257–1268. [PubMed: 18849982]

Devenport D, Oristian D, Heller E, Fuchs E. Mitotic internalization of planar cell polarity proteins preserves tissue polarity. Nat. Cell Biol. 2011; 13:893–902. [PubMed: 21743464]

Etheridge SL, Ray S, Li S, Hamblet NS, Lijam N, Tsang M, Greer J, Kardos N, Wang J, Sussman DJ, Chen P, Wynshaw-Boris A. Murine dishevelled 3 functions in redundant pathways with dishevelled 1 and 2 in normal cardiac outflow tract, cochlea, and neural tube development. PLoS Genet. 2008; 4:e1000259. [PubMed: 19008950]

Goodrich LV, Strutt D. Principles of planar polarity in animal development. Development. 2011; 138:1877–1892. [PubMed: 21521735]

Gubb D, Garcia-Bellido A. A genetic analysis of the determination of cuticular polarity during development in Drosophila melanogaster. J. Embryol. Exp. Morphol. 1982; 68:37–57. [PubMed: 6809878]

Guo N, Hawkins C, Nathans J. Frizzled6 controls hair patterning in mice. Proc. Natl. Acad. Sci. USA. 2004; 101:9277–9281. [PubMed: 15169958]

Hua ZL, Chang H, Wang Y, Smallwood PM, Nathans J. Partial interchangeability of Fz3 and Fz6 in tissue polarity signaling for epithelial orientation and axon growth and guidance. Development. 2014; 141:3944–3954. [PubMed: 25294940]

Lawrence PA, Casal J, Struhl G. Cell interactions and planar polarity in the abdominal epidermis of Drosophila. Development. 2004; 131:4651–4664. [PubMed: 15329345]

Matis M, Axelrod JD. Regulation of PCP by the fat signaling pathway. Genes & development. 2013; 27:2207–2220. [PubMed: 24142873]

Puspoki Z, Storath M, Sage D, Unser M. Transforms and operators for directional bioimage analysis: a survey. Adv. Anat. Embryol. Cell Biol. 2016; 219:69–93. [PubMed: 27207363]

Ravni A, Qu Y, Goffinet AM, Tissir F. Planar cell polarity cadherin Celsr1 regulates skin hair patterning in the mouse. J. Investig. Dermatol. 2009; 129:2507–2509. [PubMed: 19357712]

Renier N, Wu Z, Simon DJ, Yang J, Ariel P, Tessier-Lavigne M. iDISCO: a simple, rapid method to immunolabel large tissue samples for volume imaging. Cell. 2014; 159:896–910. [PubMed: 25417164]

Schneider MR, Schmidt-Ullrich R, Paus R. The hair follicle as a dynamic miniorgan. Curr. Biol. 2009; 19:R132–R142. [PubMed: 19211055]

Sennett R, Wang Z, Rezza A, Grisanti L, Roitershtein N, Sicchio C, Mok KW, Heitman NJ, Clavel C, Ma'ayan A, Rendl M. An Integrated transcriptome Atlas of embryonic hair follicle progenitors, their niche, and the developing skin. Dev. Cell. 2015; 34:577–591. [PubMed: 26256211]

Song H, Hu J, Chen W, Elliott G, Andre P, Gao B, Yang Y. Planar cell polarity breaks bilateral symmetry by controlling ciliary positioning. Nature. 2010; 466:378–382. [PubMed: 20562861]

Struhl G, Casal J, Lawrence PA. Dissecting the molecular bridges that mediate the function of Frizzled in planar cell polarity. Development. 2012; 139:3665–3674. [PubMed: 22949620]

Strutt DI. Asymmetric localization of frizzled and the establishment of cell polarity in the Drosophila wing. Mol. Cell. 2001; 7:367–375. [PubMed: 11239465]

Strutt H, Strutt D. Differential stability of flamingo protein complexes underlies the establishment of planar polarity. Curr. Biol. 2008; 18:1555–1564. [PubMed: 18804371]

Taylor J, Abramova N, Charlton J, Adler PN. Van Gogh: a new Drosophila tissue polarity gene. Genetics. 1998; 150:199–210. [PubMed: 9725839]

Usui T, Shima Y, Shimada Y, Hirano S, Burgess RW, Schwarz TL, Takeichi M, Uemura T. Flamingo, a seven-pass transmembrane cadherin, regulates planar cell polarity under the control of Frizzled. Cell. 1999; 98:585–595. [PubMed: 10490098]

Vasioukhin V, Degenstein L, Wise B, Fuchs E. The magical touch: genome targeting in epidermal stem cells induced by tamoxifen application to mouse skin. Proc. Natl. Acad. Sci. USA. 1999; 96:8551–8556. [PubMed: 10411913]

Vinson CR, Adler PN. Directional non-cell autonomy and the transmission of polarity information by the frizzled gene of Drosophila. Nature. 1997; 329:549–551.

Vladar EK, Antic D, Axelrod JD. Planar cell polarity signaling: the developing cell's compass. Cold Spring Harb. Perspect. Biol. 2009; 1:a002964. [PubMed: 20066108]

Wang Y, Badea T, Nathans J. Order from disorder: self-organization in mammalian hair patterning. Proc. Natl. Acad. Sci. USA. 2006; 103:19800–19805. [PubMed: 17172440]

Wang Y, Chang H, Nathans J. When whorls collide: the development of hair patterns in frizzled 6 mutant mice. Development. 2010; 137:4091–4099. [PubMed: 21062866]

Wang Y, Chang H, Rattner A, Nathans J. Frizzled receptors in development and disease. Curr. Top. Dev. Biol. 2016; 117:113–139. [PubMed: 26969975]

Wong LL, Adler PN. Tissue polarity genes of Drosophila regulate the subcellular location for prehair initiation in pupal wing cells. J. Cell Biol. 1993; 123:209–221. [PubMed: 8408199]

Wu J, Mlodzik M. A quest for the mechanism regulating global planar cell polarity of tissues. Trends Cell Biol. 2008; 19:295–305.

Yin H, Copley CO, Goodrich LV, Deans MR. Comparison of phenotypes between different vangl2 mutants demonstrates dominant effects of the Looptail mutation during hair cell development. PLoS One. 2012; 7:e31988. [PubMed: 22363783]

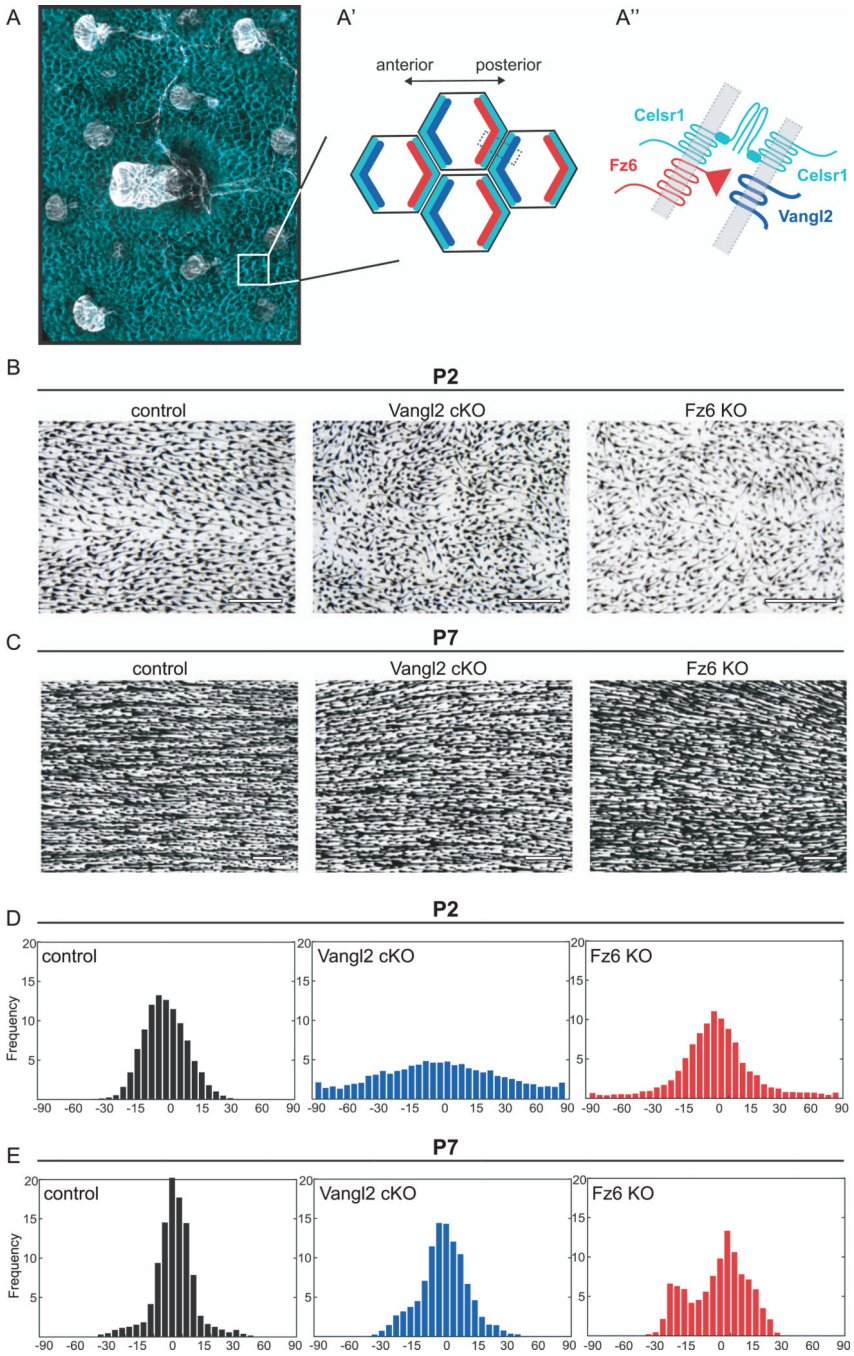


**Fig. 1.**

Disordered hair patterns in Vangl2 and Fz6 mutants correct over time. (A) Schematic of planar cell polarity in the embryonic epidermis at the tissue (A), cellular (A′) and subcellular level (A″). (A, A′) PCP proteins are localized to AP junctions where they instruct the anterior tilt of the follicle. Celsr1 is shown in cyan and hair follicles are shown in white. (A′,A″) Celsr1, Vangl2 (cyan, blue) complexes localize at the anterior cell border while Celsr1, Fz6 (cyan, red) complexes localize at the posterior cell border. These complexes interact across AP borders. (B,C) Hair follicles from wild type control, Vangl2

cKO, and Fz6 KO dorsal epidermis at P2 (B) and P7 (C). See Table 1 for specific genotypes. Skins were cleared and hair follicle pigment was imaged by bright field microscopy. Anterior is to the left in all figures. (D,E) Quantification of hair follicle orientations at P2 (D) and P7 (E). See Methods. Anterior-posterior axis = 0 degrees. Angular frequencies at P2 are pooled from control (n=6 animals); Vangl2 cKO (n=5 animals); Fz6 KO (n=3 animals). P7: controls (n=4 animals), Vangl2 cKO (n=5 animals), Fz6 KO (n=3 animals). Scale bar, 500 μm.

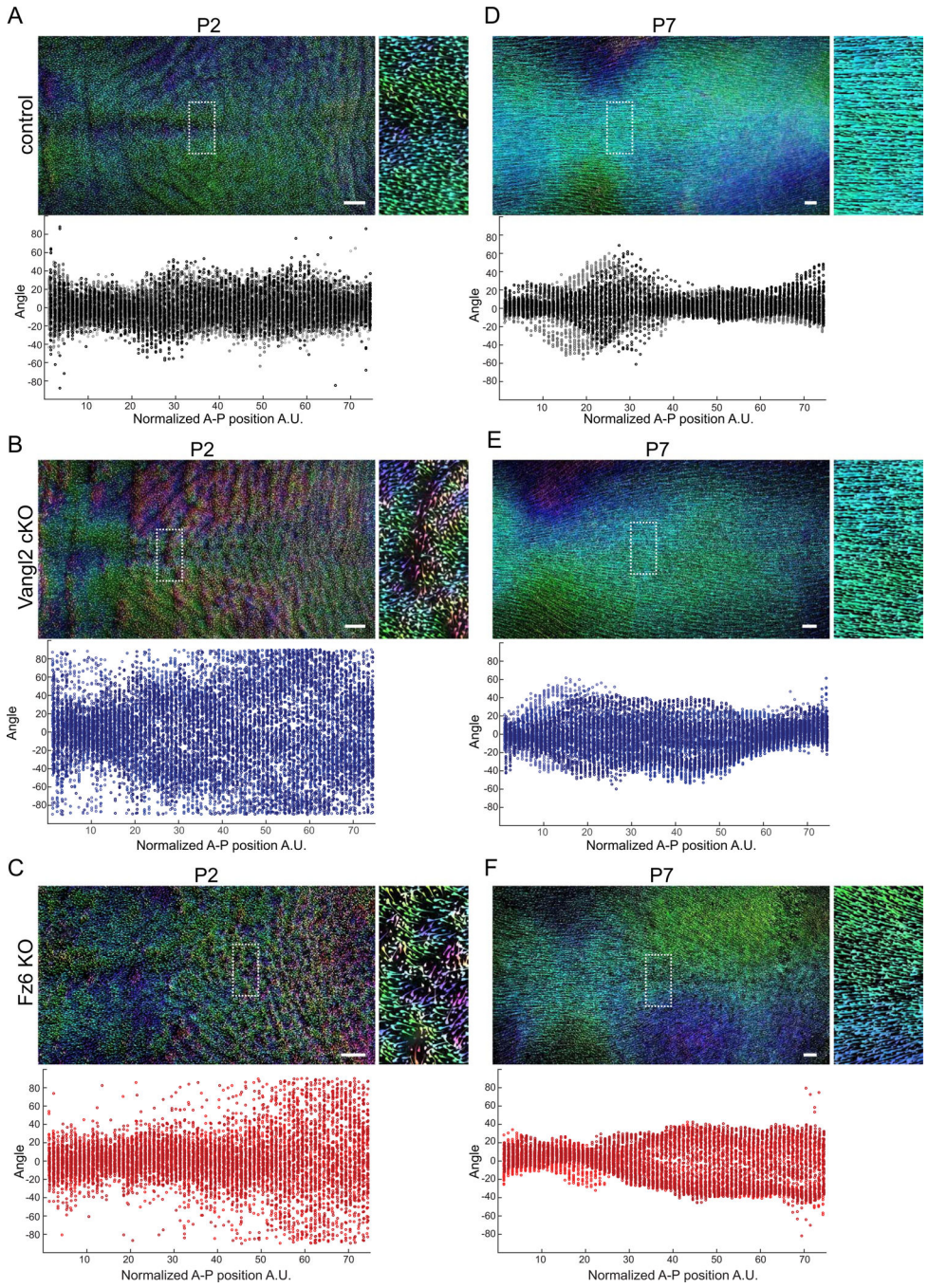


**Fig. 2.**

Postnatal hair follicle refinement is independent of Vangl2 and Fz6. (A–C) Wild type control (A), Vangl2 cKO, (B) and Fz6 KO (C) dorsal skins at P2. Hair follicles are pseudo-colored according to their angle using Orientation J. Green-blue represents hair follicles oriented closest to the AP axis ~ 0° to +/− 45°. Pink-purple ~ −45° to −90°. Orange-yellow ~ +45° to +90°. The boxed regions are shown zoomed in on the right. Quantification of hair follicle angles plotted relative to their position along the anterior-posterior axis is shown below. Each dot represents the average orientation of follicles within one square window, tiled

across the backskin. See Methods. Each color shade represents data from one animal. For control n=6, Vangl2 cKO n=5, and Fz6 KO n=3 animals. (D–F) The same analysis was carried out at P7. For control n=4, Vangl2 cKO n=5, and Fz6 KO n=3. Note that the disordered hair pattern at P2 is aligned with the anterior-posterior axis by P7. Scale bar, 1 mm.

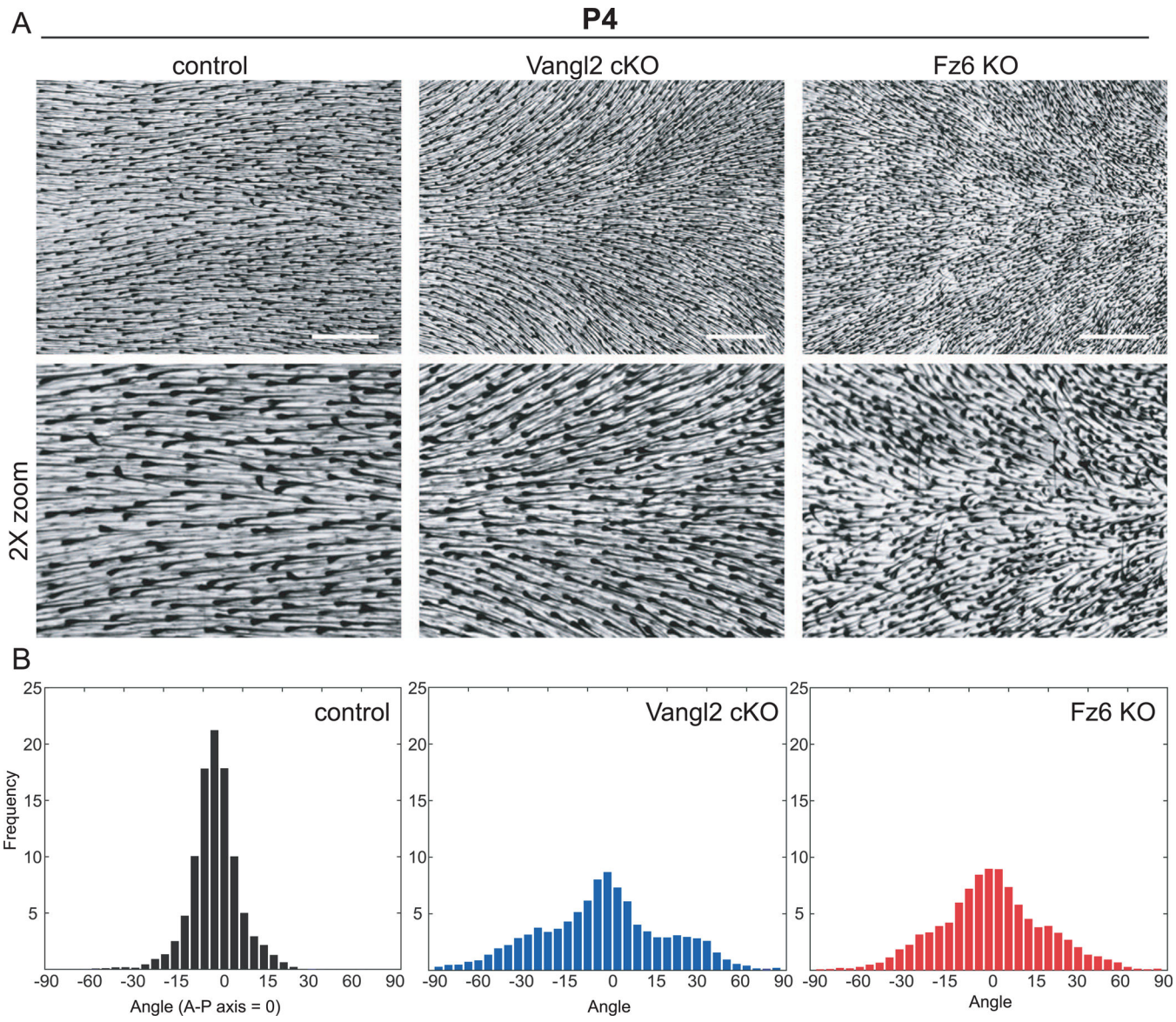


**Fig. 3.**

Stereotyped hair patterns emerge during follicle refinement. (A) Hair follicles from wild type control, Vangl2 cKO, and Fz6 KO dorsal epidermis at postnatal day 4 (P4). Skins were cleared and hair follicle pigment was imaged by bright field microscopy. Zoomed regions (2x) are shown below. (B) Quantification of hair follicle orientations at P4. Anterior-posterior axis = 0°. Frequencies are pooled from control (n=5 animals); Vangl2 cKO (n=6 animals); Fz6 KO (n=6 animals). Scale bar, 1 mm.

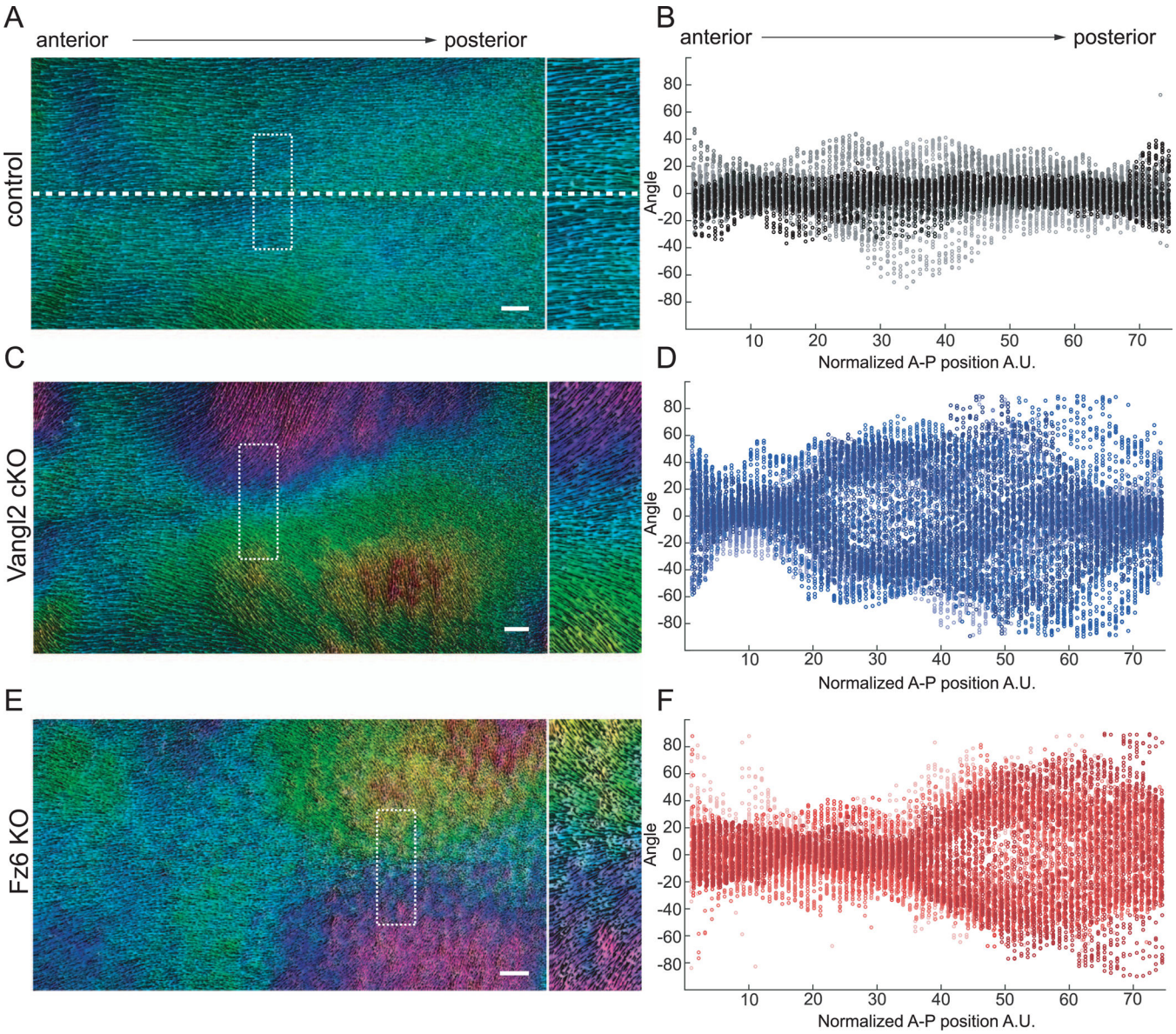


**Fig. 4.**

Vangl2 cKO and Fz6 KO follicles refine in opposing directions. (A,C,E) Wild type control (A), Vangl2 cKO (C) and Fz6KO (E) dorsal skins at P4 (left). Hair follicles are pseudo-colored according to their angle using Orientation J. Green-blue represents hair follicles oriented closest to the AP axis ~ 0° to +/− 45°, anterior-posterior axis. Pink-purple ~ −45° to −90°. Orange-yellow ~ +45° to +90°. Boxed region is shown zoomed on the right. The dotted horizontal line indicates the midline. The position of the midline is consistent across all whole backskin images. Note that while anterior-most follicles have the correct orientation in all conditions, central and posterior follicles point inward, toward the midline, in Vangl2 cKO skin (C) and outward, away from the midline, in Fz6 KO skin (E). For additional examples, see Supplemental Fig. 1. (B,D,F) Quantification of hair follicle angles plotted relative to their position along the anterior-posterior axis. Each dot represents the average orientation of follicles within one square window, which were tiled across the entire

backskin. See Section 2. Each color shade represents data from one animal. n=6 animals for control, Vangl2 cKO, and Fz6 KO. Scale bar, 1 mm.

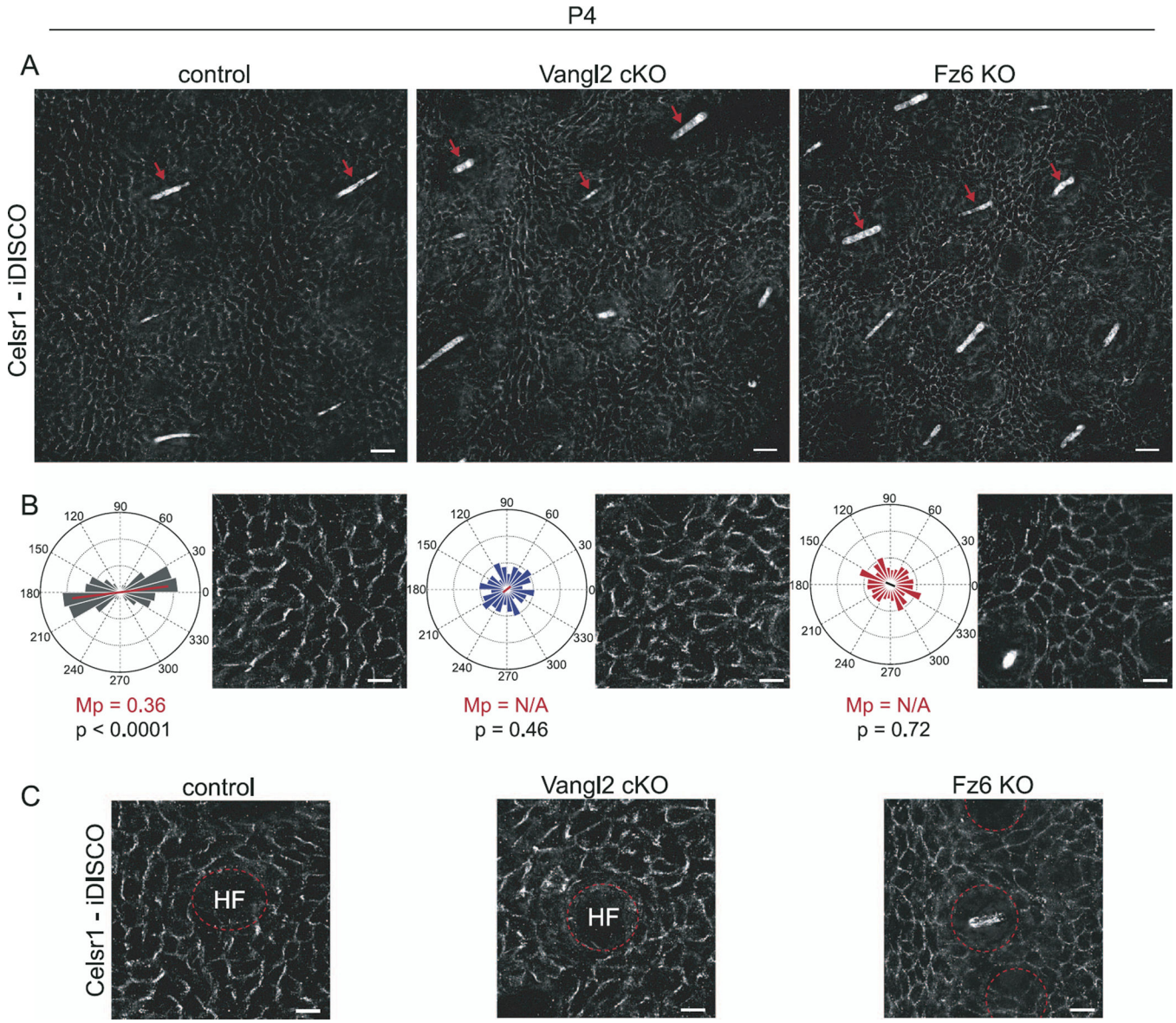


**Fig. 5.**

During refinement, hair follicle orientation is uncoupled from Celsr1 asymmetry in the interfollicular epidermis. (A) Immunofluorescence images of wild type control, Vangl2 cKO, and Fz6 KO dorsal skin at P4 labeled with antibodies against Celsr1. Tissues were cleared and processed for immunofluorescence using the iDISCO technique. Images are oriented with hairs (red arrows) aligned in the same direction. Note that despite similar follicle orientations in all three genotypes, Celsr1 is enriched at anterior-posterior borders of interfollicular epidermal cells in wild type control but not Vangl2 cKO or Fz6 KO animals. Scale bar, 25 μm. (B) Angular distribution of Celsr1 polarity in the interfollicular epidermis. Frequency scale 0 −0.3. The anterior-posterior axis runs horizontally. Control, n=1094 cells from 3 animals; Vangl2 cKO, n=1292 cells from 3 animals; Fz6 KO n=1391 cells from 3 animals. $M_P$ = magnitude of average Celsr1 polarity. The significance of the angular variation within each stage was assessed using a nonparametric permutation test. Statistical

significance = $p < 0.01$ (if $p \geq 0.01$, magnitude of average Celsr1 polarity, $M_P$ = N/A). See Methods. (C) Representative images of Celsr1 localization surrounding individual hair follicles (labeled HF). Scale bar, 10 μm.

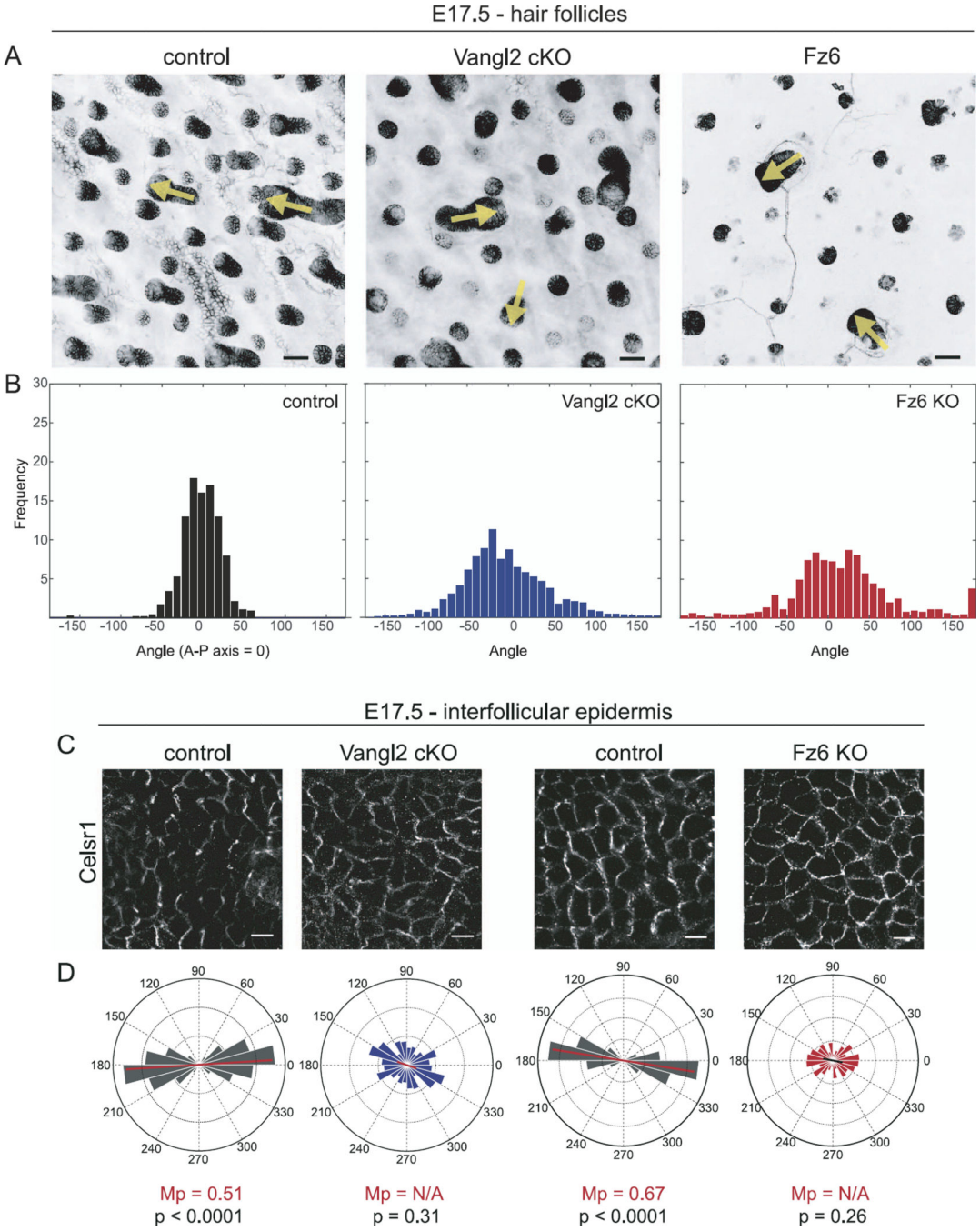


**Fig. 6.**

Uncoupling of hair follicle orientation and Celsr1 asymmetry during embryogenesis. (A) Representative hair follicles from wild type control, Vangl2 cKO, and Fz6 KO embryos at E17.5 labeled with E-Cadherin (control and Vangl2 cKO) or membrane-GFP (Fz6 KO). Yellow arrows indicate the orientation of a subset of hair follicles. See Table 1 for genotypes. Single confocal z-planes are shown. Scale bar, 50 μm. (B) Quantification of hair follicle orientations of the indicated genotypes at E17.5. Control, n=764 follicles; Vangl2 cKO, n= 1284 follicles; Fz6 KO, n= 609 follicles. (C) Representative immunofluorescence

images of Celsr1 labeled interfollicular epidermis at E17.5. Single confocal planes are shown. (D) Quantification of angular distribution of Celsr1 polarity in the interfollicular epidermis of E17.5 Vangl2 cKO (cKO, n=1083 cells from 2 embryos; control littermates n=1049 cells from 2 embryos), and Fz6 KO embryos (KO, n=948 cells from 3 embryos; control littermates, n=2184 cells from 3 embryos). Frequency scale 0–0.3 for Vangl2 pair; 0–0.4 for Fz6 pair. Scale bar, 10 μm.

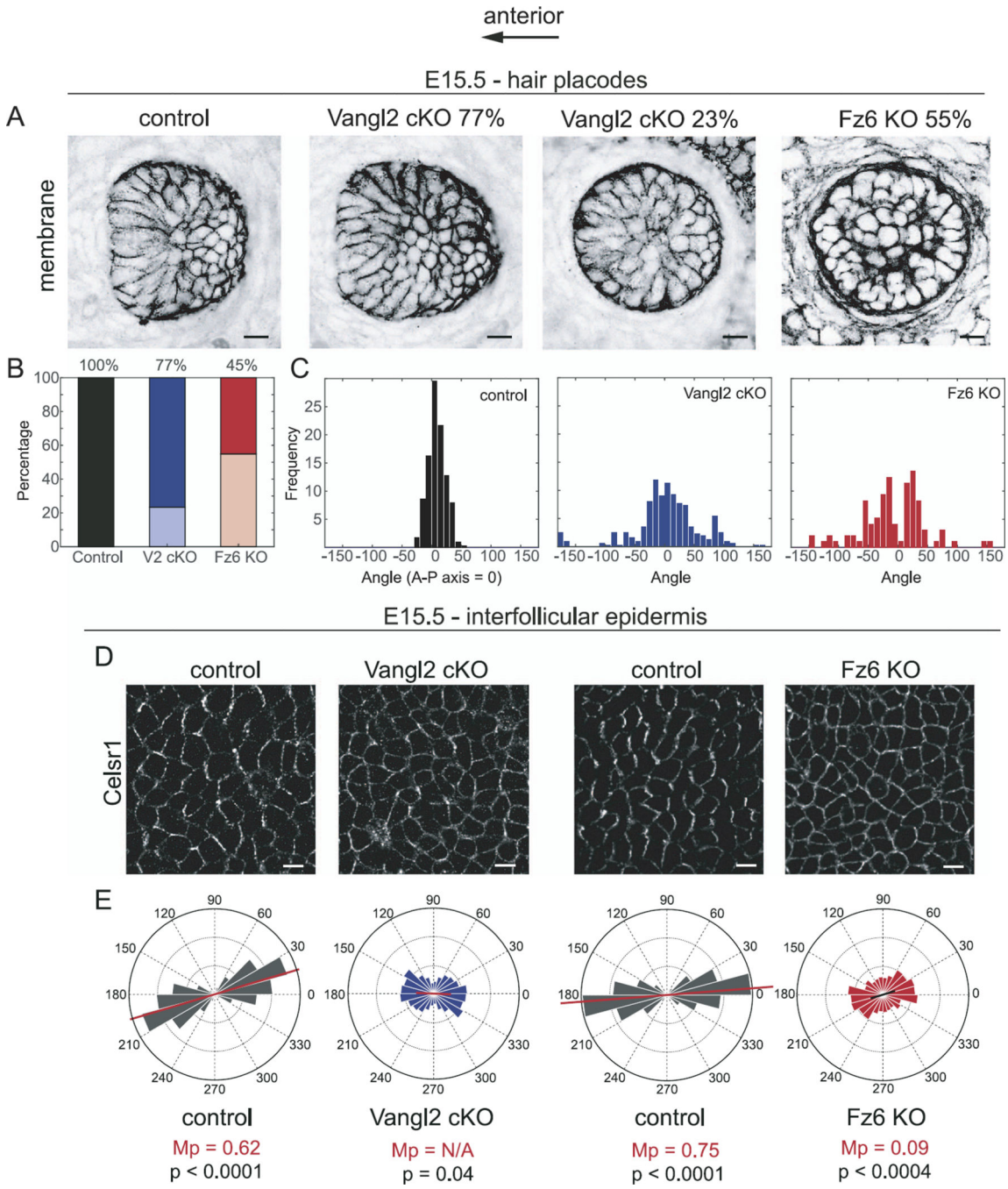


**Fig. 7.**

Relationship between hair placode orientation and Celsr1 asymmetry at initial hair follicle polarization. (A) Representative hair follicle placodes from wild type control, Vangl2 cKO (angled, left and vertical, right), and Fz6 KO embryos at E15.5 labeled with membrane-GFP (control and Vangl2 cKO) or membrane-tdTomato (Fz6 KO). See Table 1 for genotypes. Single confocal z-planes are shown. (B) Relative frequency of angled (dark shades) versus vertical (light shades) follicle placodes at E15.5. Wild type control, n= 393 follicles; Vangl2 cKO, n=406 follicles; Fz6 KO, n= 374 follicles. (C) Quantification of hair follicle

orientations of the indicated genotypes at E15.5. Only angled, not vertical, placodes are included. Wild type control, n=393 follicles; Vangl2 cKO, n=311 follicles; Fz6 KO n=181. (D) Representative immunofluorescence images of Celsr1 labeled interfollicular epidermis at E15.5. Single confocal planes are shown. (E) Quantification of the angular distribution of Celsr1 polarity in the interfollicular epidermis at E15.5 of Vangl2 cKO (cKO, n=3068 cells from 2 embryos; control littermates n=2971 cells from 2 embryos), and Fz6 KO embryos (KO, n=4076 cells from 3 embryos; control littermates, n=2994 cells from 3 embryos). Frequency scale 0-0.3. Scale bar, 10 μm.

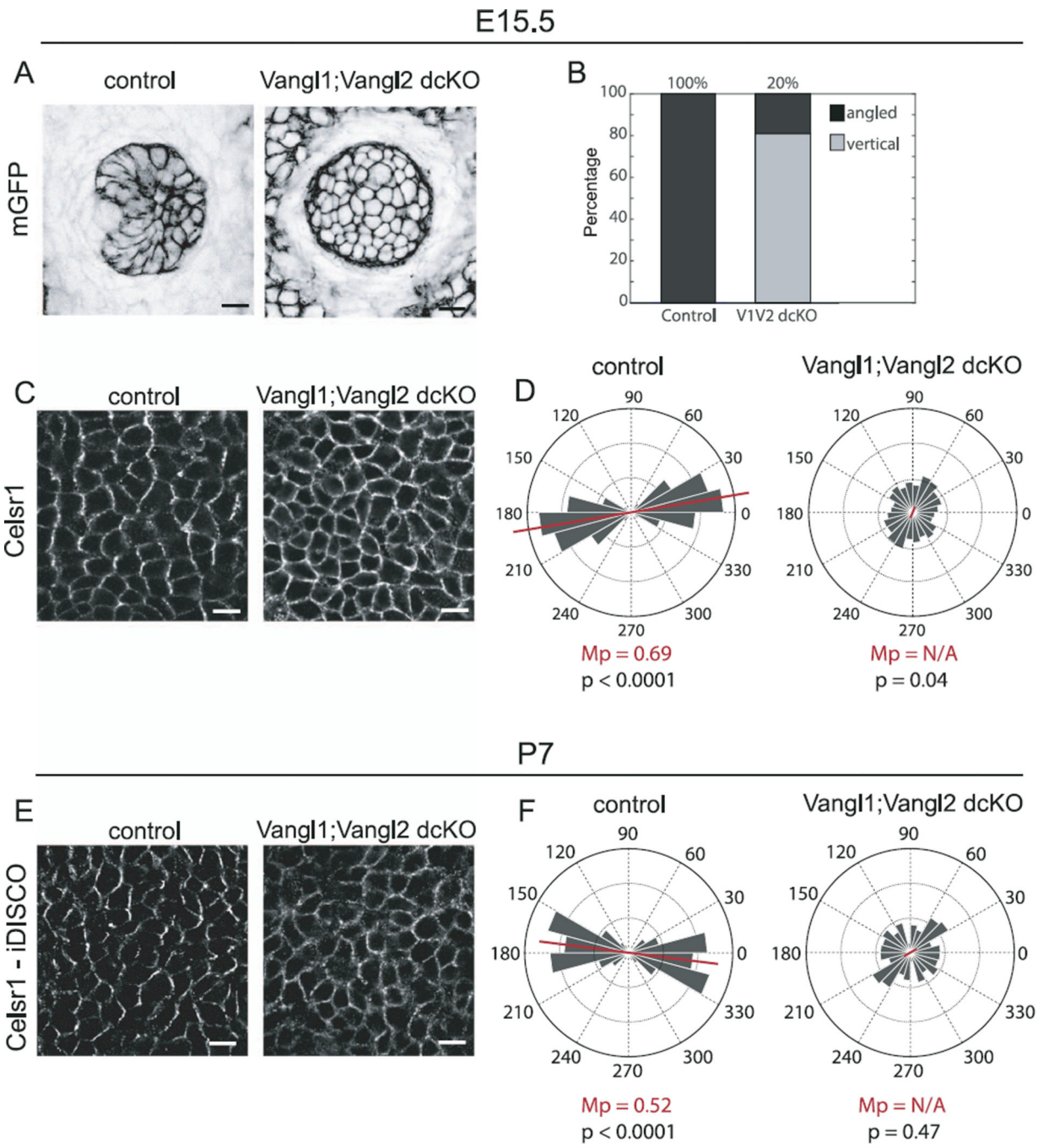


**Fig. 8.**

Loss of hair follicle polarization and Celsr1 asymmetry in Vangl1; Vangl2 dcKO epidermis. (A) Representative hair follicle placodes from wild type control and Vangl1; Vangl2 dcKO embryos at E15.5 labeled with membrane-GFP. See Table 1 for genotypes. Single confocal z-planes are shown. (B) Relative frequency of angled (dark shades) versus vertically-oriented (light shades) placodes at E15.5. The majority of Vangl1; Vangl2 dcKO placodes fail to polarize. (C) Representative immunofluorescence images of E15.5 wild type control and Vangl1; Vangl2 dcKO interfollicular epidermis labeled with Celsr1. Single confocal

planes are shown. (D) Quantification of Celsr1 polarity in the interfollicular epidermis of control and Vangl1; Vangl2 dcKO embryos. Control, n= 3533 cells from 4 embryos; dcKO, n=3111 cells from 4 embryos. (E) Immunofluorescence images of wild type control and Vangl1; Vangl2 dcKO dorsal skin at P7 labeled with antibodies against Celsr1. Tissues were cleared and processed for immunofluorescence using iDISCO. (F) Quantification of the angular distribution of Celsr1 polarity in the interfollicular epidermis at P7. (Control, n=940 cells from 3 animals, Vangl1; Vangl2 dcKO, n=987 cells from 3 animals). The anterior-posterior axis runs horizontally. Scale bar, 10 μm.

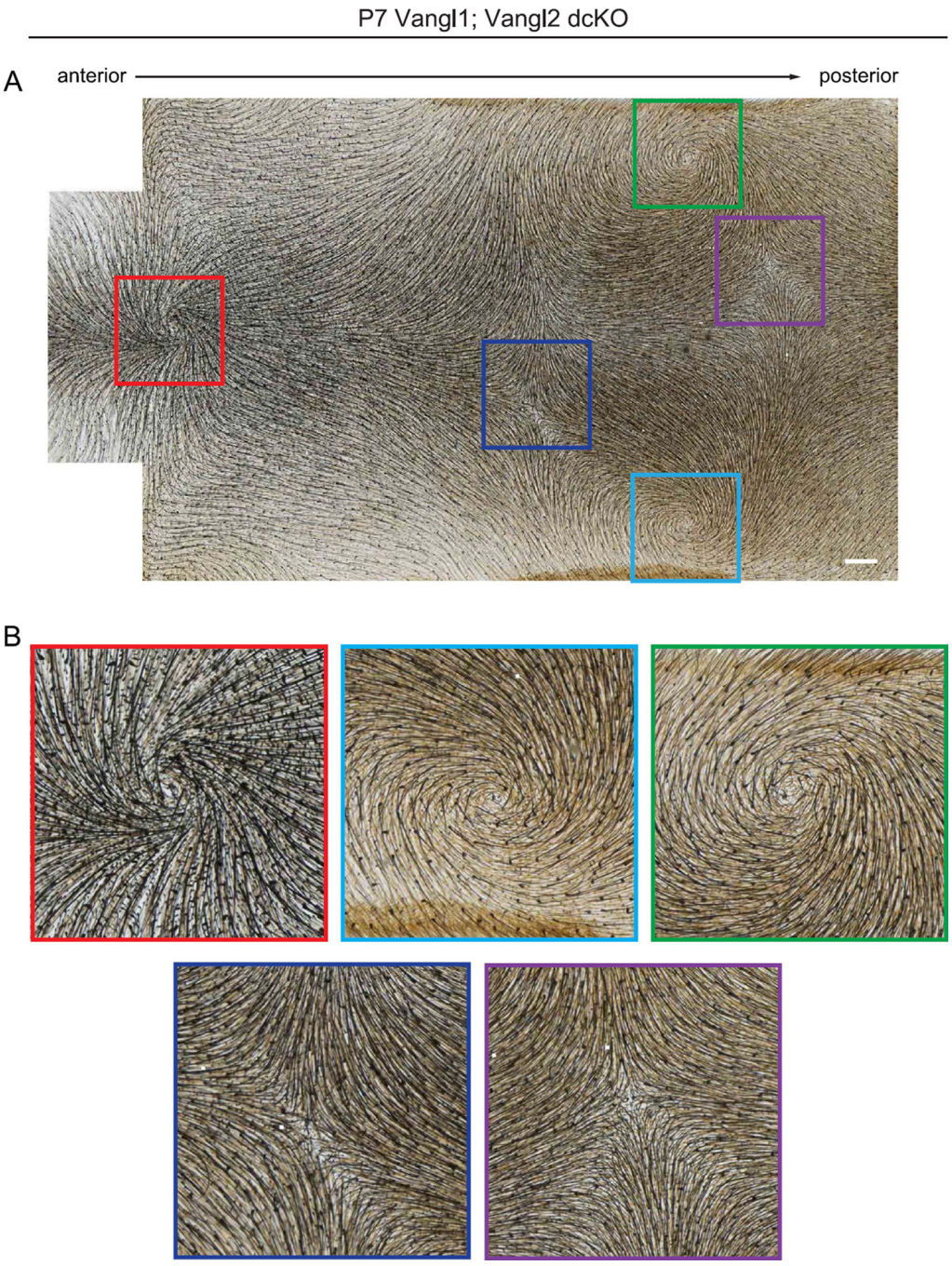


**Fig. 9.**

Stereotyped hair patterns emerge postnatally in the absence of Vangl function. (A) Representative Vangl1;Vangl2 dcKO dorsal skin at P7 showing characteristic and reproducible pattern of whorls and crosses. Note the presence of three hair whorls positioned in a triangular configuration (red, green and light blue boxes), and two crosses where whorls intersect (dark blue and purple boxes). For additional examples, see Supplementary Fig. 3. (B) Three whorls and two crosses corresponding to boxed areas in A. Scale bar, 1 mm.

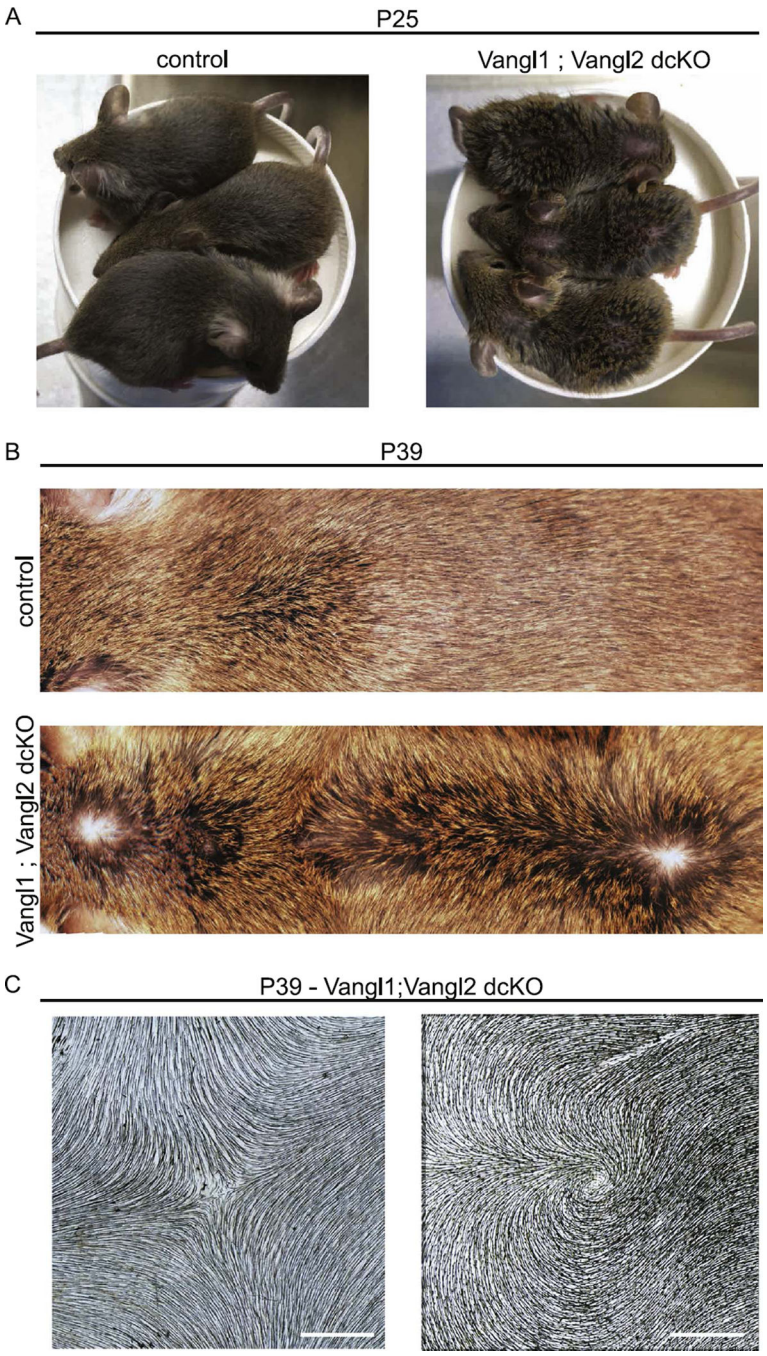


**Fig. 10.**

Hair patterns evolve over time but do not correct in the absence of Vangl function. (A) Vangl1; Vangl2 dcKO mice and their control littermates at postnatal day 25. Double knockout embryos are clearly distinguished from their control littermates due to their disorganized and scruffy hair coats. (B) Representative images of Vangl1;Vangl2 dcKO and control dorsal skin at P39. Note the presence of two hair whorls and a zone of reversal positioned along the midline. For additional examples of P39 dorsal skins, see Supplementary Fig. 4. (C) Representative hair whorl and cross from Vangl1;Vangl2 dcKO at

P39. Dorsal epidermis was cleared and imaged for hair follicle pigment by brightfield microscopy. Scale bar, 1 mm.

## Table 1

Mouse genotypes.

| Figure | Stage | Mutant Genotype | Control Genotypes |
|---|---|---|---|
| **1,2** | P2, P7 | Fz6−/−; ROSA26 mTmG/ mTmG | B6 |
| | | K14Cre/+; Vangl2 fl/ΔTMs | Vangl2 fl/fl |
| | | | Vangl2 fl/ΔTMs |
| **3,4** | P4 | Fz6−/−; ROSA26 mTmG/ mTmG | B6 |
| | | K14Cre/+; Vangl2 fl/ΔTMs | Vangl2 fl/+ |
| | | | Vangl2 fl/ΔTMs |
| **5** | P4 | Fz6−/−; ROSA26 mTmG/ mTmG | Vangl2 fl/+; mtmg/+ |
| | | K14Cre/+; Vangl2 fl/ΔTMs; ROSA26 mTmG/+ | Vangl2 fl/ΔTMs; mtmg/+ |
| **6** | e15.5 | Fz6−/−; ROSA26 mTmG/+ | Fz6+/−; ROSA26 mTmG/+ |
| | | K14Cre/+; Vangl2 fl/ΔTMs | K14Cre/+; Vangl2 fl/+ |
| **7** | e17.5 | Fz6−/−; ROSA26 mTmG/+; ShhCre/+ | Fz6+/−; ROSA26 mTmG/+ |
| | | K14Cre/+; Vangl2 fl/ΔTMs | K14Cre/+; Vangl2 fl/+ |
| **8** | e15.5 | K14Cre/+; Vangl1 fl/fl; Vangl2 | Vangl1 fl/fl; Vangl2 ΔTMs/ |
| | | fl/ΔTMs; ROSA26 mTmG/+ | +; ROSA26 mTmG/+ |
| | | | Vangl1 fl/fl; Vangl2 fl/+; ROSA26 mTmG/+ |
| | | | Vangl2 ΔTMs/+; ROSA26 mTmG/+ |
| **9** | P7 | K14Cre/+; Vangl1 fl/fl; Vangl2 | Vangl1 fl/fl; Vangl2 fl/ |
| | | fl/ΔTMs; ROSA26 mTmG/+ | ΔTMs; ROSA26 mTmG/+ |
| | | | Vangl1 fl/fl; Vangl2 fl/+; ROSA26 mTmG/+ |
| **10** | P39 | K14Cre/+; Vangl1 fl/fl; Vangl2 | Vangl1 fl/fl; Vangl2 fl/ |
| | | fl/ΔTMs; ROSA26 mTmG/+ | ΔTMs; ROSA26 mTmG/+ |